Synthetic Routes to Crystalline Complex Metal Alkyl Carbonates and Hydroxycarbonates via Sol–Gel Chemistry—Perspectives for Advanced Materials in Catalysis

Schirin Hanf [1,*,†], **Carlos Lizandara-Pueyo** [1,2], **Timo Philipp Emmert** [1], **Ivana Jevtovikj** [1], **Roger Gläser** [3] and **Stephan Andreas Schunk** [1,2,3,*]

[1] hte GmbH, Kurpfalzring 104, 69123 Heidelberg, Germany; carlos.lizandara@basf.com (C.L.-P.); timo.emmert@hte-company.de (T.P.E.); ivana.jevtovikj@hte-company.de (I.J.)

[2] BASF SE, Carl-Bosch-Str. 38, 67056 Ludwigshafen, Germany

[3] Institute of Chemical Technology, Universität Leipzig, Linnéstr. 3, 04103 Leipzig, Germany; roger.glaeser@uni-leipzig.de

[*] Correspondence: schirin.hanf@kit.edu (S.H.); stephan.schunk@hte-company.de (S.A.S.)

[†] Current address: Institute for Inorganic Chemistry, Karlsruhe Institute of Technology (KIT), Engesserstraße 15, 76131 Karlsruhe, Germany.

Abstract: Metal alkoxides are easily available and versatile precursors for functional materials, such as solid catalysts. However, the poor solubility of metal alkoxides in organic solvents usually hinders their facile application in sol–gel processes and complicates access to complex carbonate or oxidic compounds after hydrolysis of the precursors. In our contribution we have therefore shown three different solubilization strategies for metal alkoxides, namely the derivatization, the hetero-metallization and CO_2 insertion. The latter strategy leads to a stoichiometric insertion of CO_2 into the metal–oxygen bond of the alkoxide and the subsequent formation of metal alkyl carbonates. These precursors can then be employed advantageously in sol–gel chemistry and, after controlled hydrolysis, result in chemically defined crystalline carbonates and hydroxycarbonates. Cu- and Zn-containing carbonates and hydroxycarbonates were used in an exemplary study for the synthesis of Cu/Zn-based bulk catalysts for methanol synthesis with a final comparable catalytic activity to commercial standard reference catalysts.

Keywords: metal alkoxides; sol–gel synthesis; methanol synthesis; solubilization techniques; CO_2 insertion

1. Introduction

Metal alkoxides are compounds of the form $M(OR)_n$ (M = metal, R = alkyl rest) and can be regarded as versatile single-source precursors for inorganic functional materials [1–9] and pre-formed solid-state entities at the molecular scale [10,11]. Through alkoxides, access can be granted to a variety of amorphous or phase-pure oxides via metal organic chemical vapor phase epitaxy (MOVPE), thermal decomposition or sol–gel processes [12–14]. The resulting metal oxides have found very wide applications in, for example, solar cells [15], batteries [16], transistors [17], supercapacitors [18] and superconductors [19], among others.

The physical properties of metal alkoxides are greatly influenced at the molecular level, i.e., the choice of metal and the nature and number of the alkyl groups R present in the molecule. Due to the strong binding within the M-O-M motif, metal alkoxides, especially transition metal alkoxides, tend to form oligomeric structures (Figure 1), which significantly reduce the solubility of the alkoxides in most organic solvents. Whereas Group IV metal alkoxides exhibit an extremely high solubility in a range of organic solvents [12], transition metal alkoxides incorporating Fe, Ni or Cu are almost insoluble in any organic solvent. Obviously, this lack of solubility hinders precise chemical modification and poses hurdles to their suitability as soluble precursors for sol–gel processes. However, the quasi-polymeric

character can be suppressed to a certain extent via steric and electronic tuning of the alkoxide OR rest [20–25]. Additionally, the solubility can be greatly influenced through the implementation of pendant donor groups (e.g.,OC_2H_4OMe or $OC_2H_4NMe_2$) [26] or via the formation of multimetallic alkoxides [20]. However, by using the mentioned modification approaches [27], the inherent stoichiometric limitations can hardly be overcome.
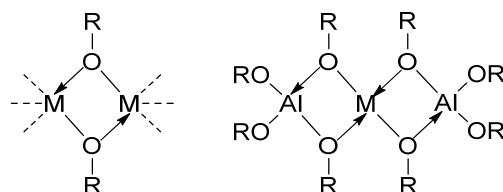
Figure 1. Schematic representation of the formation of oligomeric alkoxides via oxygen bridging.

Depending on whether one or more types of metal cations are involved in the corresponding alkoxides, compounds are referred to as homometallic or heterometallic alkoxides, both of which [28] are highly reactive compounds due to the strongly polarized $M^{\delta+}$-$O^{\delta-}$-C bond, and, consequently, require handling under inert conditions. Whereas the oxygen atom is likely to react with electrophilic reagents, the metal center is prone to nucleophilic attack, for example, by water, whereby the reaction follows a complex sequence of hydrolysis and condensation reactions (Scheme 1) [29]. During the hydrolysis, the alkoxide groups are either replaced by hydroxo (OH^-) or oxo (O^{2-}) ligands. In the presence of sufficient amounts of water and $x \leq 2$, other nucleophilic attacks of water take place. Subsequently, the M-O-M chain is prolonged, and the sol–gel process starts. In excess water, the simultaneous nucleophilic attack of water on all alkoxy groups takes place and leads to the formation of solvated metal hydroxides. The final product of the hydrolysis is the formation of complex oxidic or typically amorphous hydroxy-based solids.
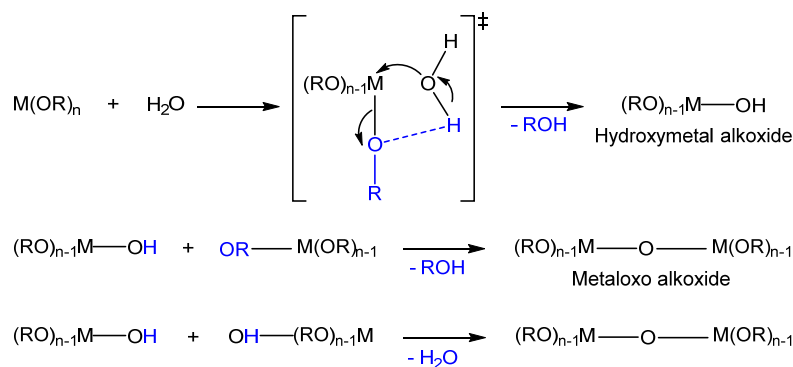
Scheme 1. Stepwise hydrolysis of metal alkoxides and the formation of hydroxy metal alkoxides and metal oxo alkoxides (R: alkyl rest) [5,29].

As well as the reactivity of metal alkoxides towards water, the reaction of metal alkoxides with small molecules, such as CO_2, has been investigated in the past (Scheme 2). Computational studies suggest that the electron lone pair on the oxygen atom of the metal alkoxide acts as a nucleophile and attacks the carbon atom of CO_2, resulting in a zwitterionic intermediate. This intermediate then rearranges in a rate determine step, resulting in a new M-O bond [30]. Lastly, the cleavage of the corresponding metal alkoxide M-OR bond takes place to give the metal mono-alkyl carbonate (MMAC) product [31]. The formation of metal mono-alkyl carbonates is not only described for alkali metal-based alkoxides, but also known for Ti-, Zr-, Fe-, Nb-, Mo- and Cu-based alkoxides [32–34]. However, in the case of transition metal-based MMACs, the isolation of pure materials has rarely been reported and often only spectroscopic evidence is given for their formation. As well as the challenges involved in the isolation of pure metal alkyl carbonates, the potential of the CO_2 insertion into the M-O bond of metal alkoxides is utilized in a variety

of catalytic transformations, such as in ring-opening polymerizations, ring-opening co-polymerizations and transesterification reactions. Hereby, it was found that metal alkoxides can be employed as catalysts for the preparation of polyoxygenates [35].
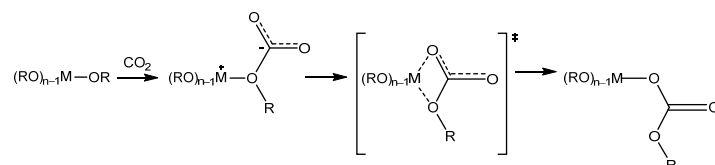
Scheme 2. Reaction of metal alkoxides with CO_2 leading to metal alkyl carbonates (R: alkyl rest) [30].

Spurred on by the possibility of adjusting the reactivity, solubility and composition of metal alkoxides at the molecular level, we investigated the utilization of metal alkoxides as precursors for advanced functional materials in catalysis. However, to exploit the full potential of metal alkoxides and to make them widely accessible for sol–gel chemistry, the solubility of many homometallic alkoxides must be tremendously enhanced. Therefore, we explored various solubilization strategies of metal alkoxide precursors, such as the derivatization via alcohol exchange reactions, the hetero-metallization and the CO_2 insertion to obtain metal alkyl carbonates. Although such carbonate species have been described in the context of polymerization catalysis before, we present them as alternative precursors for sol–gel synthesis for the first time. Whereas metal oxides or hydroxides are usually used as the source for sol–gel materials, [13] the utilization of metal alkyl carbonates can give rise to new materials, also for catalytic applications. Hereby, the amount of water for the hydrolysis reaction and the addition of a cosolvent can give control over the meso-structures of the resulting materials.

2. Results and Discussion

2.1. Solubilization Strategies of Metal Alkoxide Precursors

Based on the high solubility of organometallic precursors in various organic solvents and their controllable reactivity, organometallic compounds have widely been reported as single-source precursors for the synthesis of ceramic and oxidic materials [36]. However, the complex multi-step synthesis of such organometallic precursors makes them unsuitable precursors in the scope of this work. Moreover, when using organometallic compounds, safety aspects must be considered, especially with respect to upscaling for application in the chemical industry. Therefore, our devised strategy to synthesize solid oxidic catalysts is the widely reported sol–gel approach [37–42] in combination with tailor-made metal alkoxide systems, which are usually insoluble. As the solubility and reactivity of the starting materials have been demonstrated as being crucial to fine-tune the properties of the final materials when sol–gel processes are used, in the current work, we have employed the three following strategies to break the polymeric structure of the easily available and versatile metal alkoxide precursors (Figure 2):

(a) Derivatization (alcohol exchange)
(b) Hetero-metallization
(c) CO_2 insertion
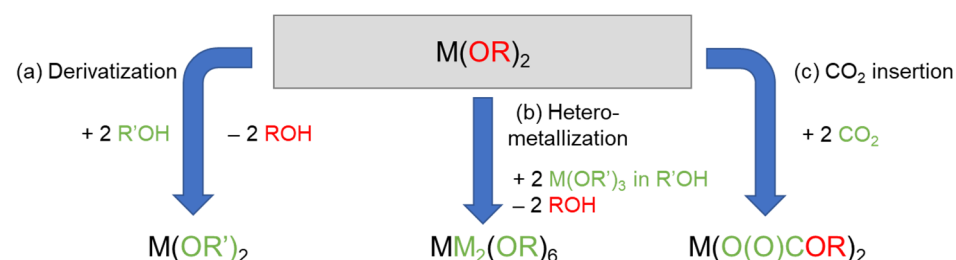
Figure 2. Solubilization strategies for metal alkoxides (R: alkyl rest).

All these strategies have yielded soluble precursors in organic solvents that have allowed us to synthesize nanomaterials with controlled size, composition, and nano- and meso-structure. Noteworthy to mention here is that while derivatization and hetero-metallization are well known procedures reported in the literature, [43–45] the use of CO_2 insertion to solubilize metal alkoxides, is a fully new approach in the context of sol–gel chemistry. This elegant path enables the synthesis of soluble metal alkyl carbonates from insoluble metal precursors, which can then easily be utilized for the synthesis of sol–gel materials.

(a) Derivatization

The derivatization strategy gives the possibility to exchange the alkoxide group with alcohols that have a higher boiling point than the respective alcohol of the alkoxide rest present in the precursor. To verify the effectiveness of the alcohol exchange reaction, a set of experiments was performed and the future exchange alcohol ($mROH_{free}$) and the theoretically bound alcohol ($mROH_{bound}$) in the alkoxide were quantified (Table 1). Due to the identical molar masses, the exchange factor (EF) can be defined as $EF = mROH_{free}/mRO_{bound}$. It was shown that a complete replacement of the alkoxide group occurs for all metal alkoxides studied. Interestingly, the broad applicability of 2-(2-methoxyethoxy)ethanol for all metals tested indicates that this alkoxide rest allows an easy adjustment of the desired molar metal ratio of the final material at the molecular scale. Moreover, the resulting metal alkoxides were soluble in the same alcohol and several organic solvents.

Table 1. Derivatized alkoxides. EF > 0.95 in all alkoxides (OMEE: 2(2-methoxyethoxy)ethanol, OME: 2-methoxyethanol).
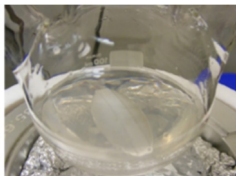
	Derivatized Alkoxide $M(OR')_n$	Starting Alkoxide $M(OR)_n$	Exch. Alcohol R'OH
1	$Al(OHex)_3$	$Al(O^iPr)_3$	1-Hexanol
2	$Al(OMEE)_3$	$Al(O^iPr)_3$	OMEE
3	$Mg(OHex)_2$	$Mg(OEt)_2$	1-Hexanol
4	$Mg(OMEE)_2$	$Mg(OEt)_2$	OMEE
5	$Zr(OMEE)_4$	$Zr(O^nPr)_4$	OMEE
6	$Ti(OMEE)_4$	$Ti(O^nPr)_4$	OMEE
7	$Cu(OMEE)_2$	$Cu(O^iPr)_2$	OMEE
8	$Zn(OMEE)_2$	$Zn(O^iPr)_2$	OMEE
9	$Zn(OME)_2$	$Zn(O^iPr)_2$	OME
10	$Co(OMEE)_2$	$Co(O^iPr)_2$	OMEE
11	$Mn(OMEE)_2$	$Mn(OMe)_2$	OMEE

(b) Hetero-metallization

As a second solubilization strategy, the formation of heterometallic alkoxides was exploited. However, this strategy is only applicable if the additional heteroatom functionality is needed in the final material. Additionally, the solubilization of the resulting alkoxide is strongly dependent on the oxidation state of the metal alkoxide that will be solubilized. In a series of experiments, various alkoxides were solubilized in the presence of 1-hexanol and $Al(OHex)_3$. After adding $M(OR)_2$ to the $Al(OHex)_3$-1-hexanol mixture and heating the samples to reflux temperature of 1-hexanol, a homogeneous slightly colored solution was formed with all heterometallic compositions shown in Table 2.

Table 2. Heterometallic alkoxides, $n[M(OR)_2]$ = 30 mmol, $n[Al(OHex)_3]$ = 60 mmol and $n[1\text{-hexanol}]$ = 300 mmol. All compositions are formed 5–10 min after reaching T = 353 K. Photographs are shown exemplarily.

	Starting Alkoxide M(OR)$_n$	Heterometallic Alkoxide M[Al(OHex)$_4$]$_z$
1	Mg(OEt)$_2$	Mg[Al(OHex)$_4$]$_2$
2	Cu(O^{i}Pr)$_2$	Cu[Al(OHex)$_4$]$_2$
3	Zn(O^{i}Pr)$_2$ Zn(O^{i}Pr)$_2$ (solid) and Al(O-Hex)$_3$ (liquid) shortly after adding the Zn(O^{i}Pr)$_2$	Zn[Al(OHex)$_4$]$_2$ After 5min formation of soluble Zn[Al(OHex)$_4$]$_2$
4	Co(O^{i}Pr)$_2$	Co[Al(OHex)$_4$]$_2$ Soluble Cu[Al(OHex)$_4$]$_2$
5	Mn(OMe)$_2$	Mn[Al(OHex)$_4$]$_2$

(c) CO$_2$ insertion

As mentioned before, the insertion of CO$_2$ is known for many metal alkoxides. However, we utilize the metal alkyl carbonates for the first time as precursors for sol–gel chemistry [32–34]. Table 3 shows the results of the solubilization of different Cu alkoxides via CO$_2$ insertion. For the insertion experiments, CO$_2$ was bubbled into a suspension of primary, secondary and tertiary Cu alkoxides in different solvents. Interestingly, the CO$_2$ insertion took place in different organic solvents and independently of the alkoxide rest. The only exceptions were non-polar and non-coordinating solvents, such as *n*-hexane, where the solubilization was not successful.

Table 3. CO$_2$ inserted alkoxides, $n[M(OR)_2]$ = 3 mmol, $V[CO_2]$ = 0.25 L·min^{-1} and $n[\text{solvent}]$ = 300 mmol, T = 313 K.

Alkoxide	Solvent	Time until Solubilized
Cu(O^{i}Pr)$_2$	^{n}Hexane	Not solubilized
Cu(O^{i}Pr)$_2$	Pyridine	0.2 h
Cu(O^{t}Bu)$_2$	^{t}Butanol	1.3 h
Cu(O^{i}Pr)$_2$	THF	1.8 h
Cu(O^{i}Pr)$_2$	^{i}Propanol	2.1 h
Cu(OMe)$_2$	Methanol	3.5 h

Apart from the fact that the copper alkoxides were solubilized through the reaction with CO$_2$, the success of the CO$_2$ insertion into various metal alkoxides was further confirmed by IR spectroscopic analyses for different solubilized alkoxides. Hereby, typical absorption bands of metal alkyl carbonates with signals at around 1625 cm^{-1}, which are attributable to C=O bond stretching and several peaks at wavenumbers of

1372 cm^{-1}, 1100 cm^{-1} and 1088 cm^{-1}, that are associated with C-O bond stretching, were observed (Figure 3).
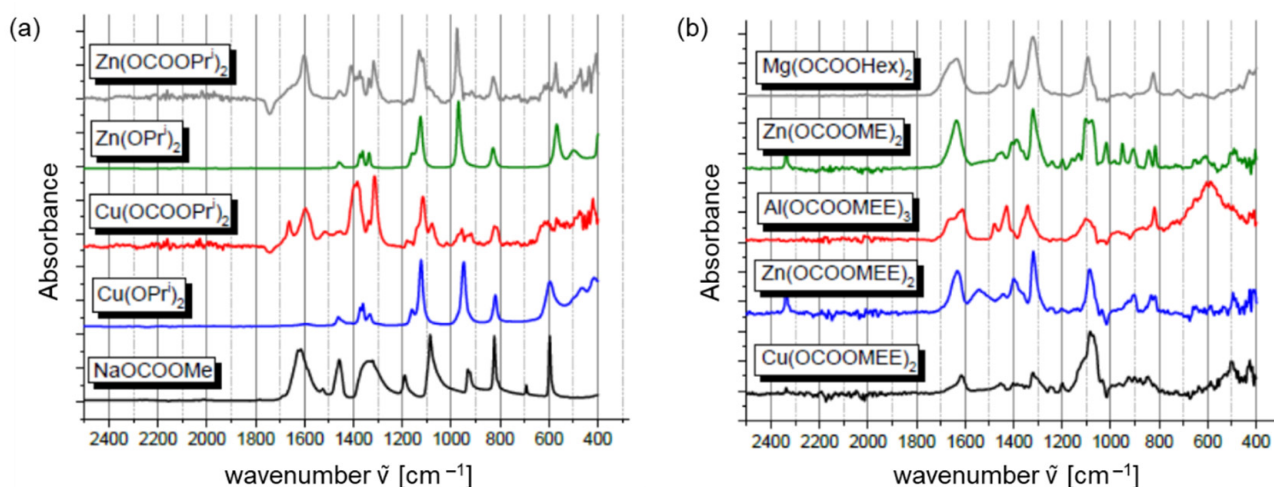
Figure 3. (**a**) ATR-IR absorption spectra of Zn(O(O)CO^{i}Pr)$_2$, Zn(O^{i}Pr)$_2$, Cu(O(O)CO^{i}Pr)$_2$, Cu(O^{i}Pr)$_2$ and Na(O(O)COMe). (**b**) ATR-IR absorption spectra of Mg(O(O)COHex)$_2$, Zn(O(O)COME)$_2$, Al(O(O)COMEE)$_3$, Zn(O(O)COMEE)$_2$ and Cu(O(O)COMEE)$_2$ between 2500–400 cm^{-1} (OMEE = 2 (2-methoxyethoxy)ethanol, OME = 2-methoxyethanol).

In order to confirm the IR results further, NMR spectroscopic studies of Mg[Al(O^{i}Pr)$_4$]$_2$ before and after the insertion of ^{13}C-enriched CO$_2$ were carried out in d$_6$-DMSO (Figure 4). After the insertion, two new peaks at 156.6 and 159.0 ppm become obvious in the ^{13}C NMR spectrum, as well as a peak for free CO$_2$, which verifies the formation of alkyl carbonate groups (O-CO$_2$) and, therefore, metal alkyl carbonates [46]. The broadening and splitting of the peaks are interpreted to be due to the non-equivalent chemical environments of the O-CO$_2$ group within a heterometallic alkyl carbonate.
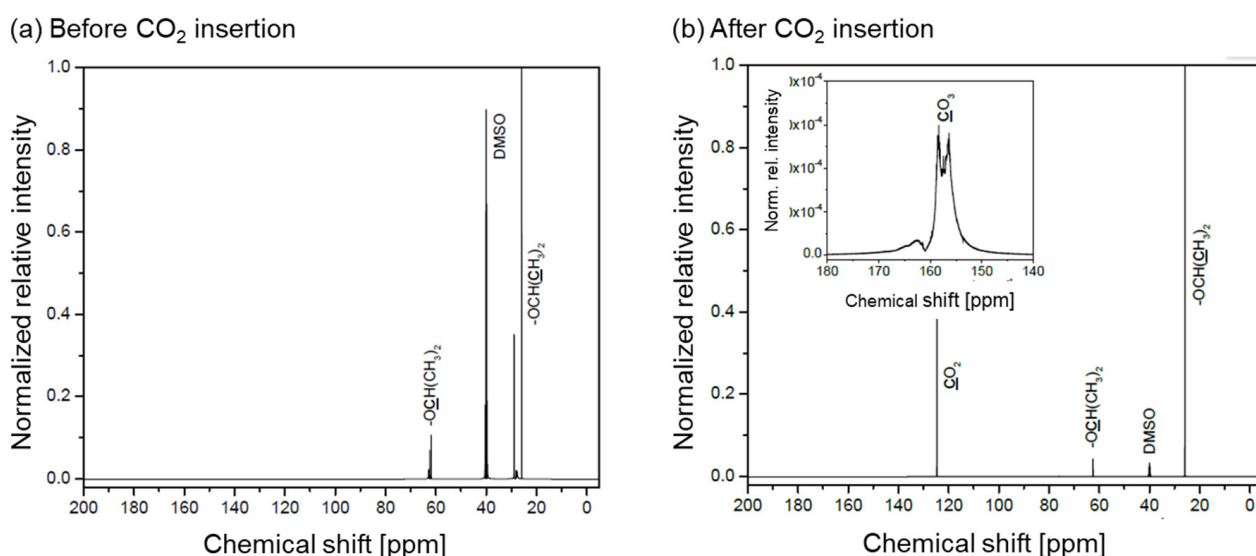
Figure 4. (**a**) ^{13}C-NMR spectrum of Mg[Al(O^{i}Pr)$_4$]$_2$ dissolved in d$_6$-DMSO before CO$_2$ insertion. (**b**) ^{13}C-NMR spectrum of Mg[Al(O^{i}Pr)$_4$]$_2$ dissolved in d$_6$-DMSO after CO$_2$ insertion. The signal at 125 ppm can be attributed to dissolved CO$_2$.

The amount of inserted CO$_2$ was quantified via a simple CO$_2$-adsorption experiment. The insoluble Cu(O^{i}Pr)$_2$ was used as a test case, which was transformed to Cu(O(O)CO^{i}Pr)$_2$ after CO$_2$ was inserted. The fully solubilized Cu(O(O)CO^{i}Pr)$_2$ solution was then treated

with a flow of argon, which led to the release of the inserted CO_2 and subsequent precipitation of the starting material $Cu(O^iPr)_2$. The released CO_2 was captured and added to a solution of $Ba(OH)_2$ leading to the formation of $BaCO_3$ and water. From the mass of dry isolated $BaCO_3$, it was confirmed that CO_2 inserts quantitatively. The same procedure was carried out for several alkoxides to calculate the so-called insertion factor (IF), determined with the given formula: $IF = nCO_2/nOR$ (Table 4). Deviations from the ideal insertion factor (IF = 1) were seen in all metal alkoxides, which most likely resulted from the incomplete adsorption of CO_2 in the washing solution. Regarding experimentally determined Cu- and Zr-insertion factors, there is a high conformity of the values published in the literature [32,34]. However, $Al(O^iPr)_3$ (see Table 4, entry 3) shows a clear difference from the ideal insertion factor, which points towards the fact that only two of the three existing alkoxy groups are accessible for an insertion reaction. Moreover, it was demonstrated that glycol ether alkoxides (see Table 4, entry 5–9) are converted to metal alkyl carbonates much faster than the solid alkoxides. Hereby, the insertion was completed after only 1 h vs. 6 h in the case of ^iPrOH alkoxides. The reason for this is most likely the liquid nature of these alkoxides that facilitates the CO_2 insertion to form the metal carbonate precursor.

Table 4. Insertion factor for different metal alkoxides, n[alkoxide] = 40 mmol, $V[CO_2] = 2$ L·min^{-1}, n[solvent] = 6 mol, T = 313 K.

	Starting Alkoxide M(OR)$_n$	Solvent	t_{CO2} (h)	IF	Formulae of Compound Based on CO_2 Adsorption Experiment
1	$Cu(O^iPr)_2$	^iPrOH	6	0.93	$Cu(O(O)CO^iPr)_{1.86}(O^iPr)_{0.14}$
2	$Zn(O^iPr)_2$	^iPrOH	6	0.89	$Zn(O(O)CO^iPr)_{1.78}(O^iPr)_{0.22}$
3	$Al(O^iPr)_3$	^iPrOH	6	0.65	$Al(O(O)CO^iPr)_{1.95}(O^iPr)_{1.05}$
4	$Zr(OPr)_4$	^nPrOH	6	0.94	$Zr(O(O)COPr)_{3.76}(OPr)_{0.24}$
5	$Cu(OMEE)_2$	OMEE	1	0.88	$Cu(O(O)COMEE)_{1.76}(OMEE)_{0.24}$
6	$Zn(OMEE)_2$	OMEE	1	0.84	$Zn(O(O)COMEE)_{1.68}(OMEE)_{0.32}$
7	$Zn(OME)_2$	OME	1	0.96	$Zn(O(O)COME)_{1.92}(OME)_{0.08}$
8	$Al(OMEE)_3$	OMEE	1	0.82	$Al(O(O)COMEE)_{2.46}(OMEE)_{0.54}$
9	$Zr(OMEE)_4$	OMEE	1	0.90	$Zr(O(O)COMEE)_{3.6}(OMEE)_{0.4}$

2.2. Hydrolysis of Metal Alkoxides

Metal hydroxides, carbonates and hydroxycarbonates are important precursors for metal oxides, which have found numerous applications [15–19]. In this context, layered double hydroxides (LDHs) have attracted considerable attention, with [47,48] LDHs consisting of positively charged brucite-like layers together with charge-balancing anions and water. LDHs are often referred to as hydrotalcite (HTC), which is a layered double hydroxide of the general formula $Mg_6Al_2CO_3(OH)_{16}\cdot4(H_2O)$, since this mineral was one of the first well-characterized examples of an LDH [49]. HTCs can be synthesized starting from a mixture of aluminum and magnesium alkoxides, which is subsequently hydrolyzed in a controlled manner to afford the solid material after filtration and washing.

To obtain an aluminum magnesium alkoxide mixture, we applied the derivatization strategy (Figure 5) and reacted magnesium ethoxide and aluminum *iso*-propoxide with 1-hexanol to afford $Mg(OHex)_2$ and $Al(OHex)_3$ (and probably also mixed metal alkoxides). Through distillative removal of the low boiling alcohols, ethanol and *iso*-propanol, full conversion could be achieved (see Figure 5). In order to obtain the corresponding HTC, two separate strategies have been developed (see Figure 5, Strategy A and B). Within strategy A, the carbonate source is added to the metal alkoxide solution by directly adding CO_2 to the molecular precursor (see Figure 5, Strategy A). In the second case, the metal alkoxide is hydrolyzed with $(NH_4)_2CO_3$, as a carbonate source, using a cosolvent strategy (see Figure 5, Strategy B).
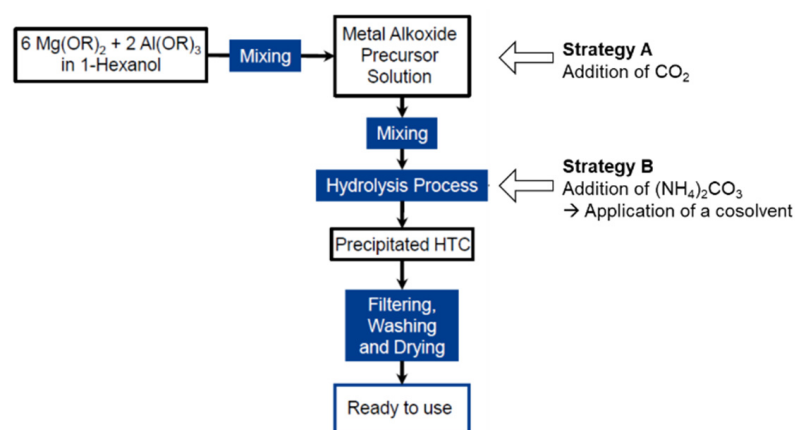
Figure 5. Schematic representation of the synthesis of LDHs from alkoxides via an alcohol exchange reaction and subsequent hydrolysis. As carbonate sources, either CO_2 (Strategy A) or $(NH_4)_2CO_3$ (Strategy B) can be utilized. (R: alkyl rest).

The second strategy B (Figure 6) was not simply used to introduce carbonate, but also to control the particle formation into a homogeneous system instead of a 2-phase system prior to nucleation. Therefore, only strategy B was considered for the following HTC syntheses and the cosolvent study.
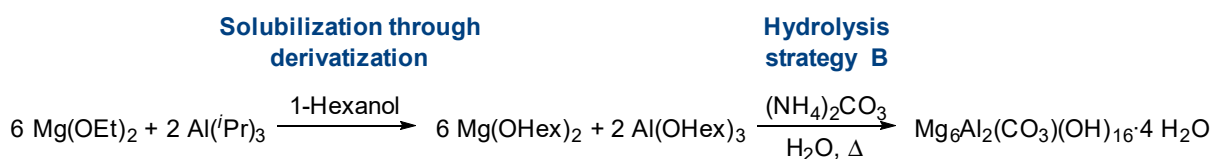
Figure 6. Simplified synthesis of HTCs using an aqueous $(NH_4)_2CO_3$ solution for the hydrolysis process (Strategy B).

Due to the low solubility of water in 1-hexanol, a 2-phase system is formed during the hydrolysis reaction, which causes only a very small temporal oversaturation through which only low amounts of nucleation seeds are present. Subsequently the hydrolysis tends to result in the formation of large particles. To avoid this 2-phase system, a third solvent, such as methanol or ethanol, which is miscible with 1-hexanol and water, can be added. Through the addition of such a cosolvent, the formation of a homogeneous mixture in an appropriate stoichiometric area is guaranteed and the hydrolysis rate is not dependent on the mass transport between the organic and water phase anymore. Therefore, the influence of the variation in the cosolvent during the hydrolysis reaction of the Mg-Al(OHex) mixture on the specific surface area and the crystallite size was investigated as depicted in Figure 7 (see ESI for further information in Supplementary Materials). It becomes obvious that the addition of a cosolvent leads to an increase in specific surface area, whereby this effect is more pronounced in the case of methanol. Additionally, the application of a cosolvent affects the crystallite size and the corresponding intensity ratio. Hereby, the effect is more evident for the crystallite size along d(003), instead of the crystallite size along d(012). In the case of ethanol, the crystallite size along d(003) is reduced to 9 nm, whereas when methanol is added to the hydrolysis mixture a further decrease to 7.5 nm becomes obvious. Through the use of a cosolvent, the I(012)/I(003) ratio is decreased, whereby again this effect is more pronounced in the case of methanol. The different results obtained for methanol and ethanol point towards some kind of interaction between the cosolvent and the forming HTC.
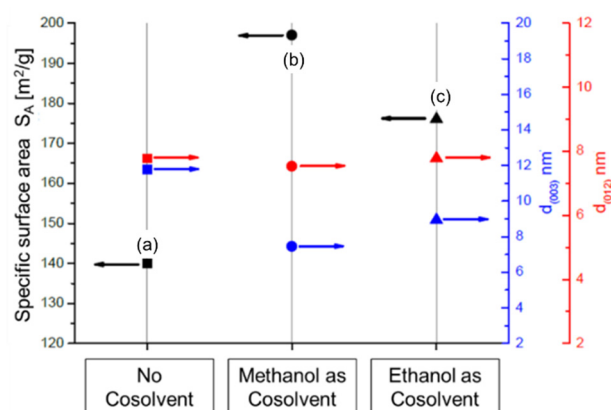
Figure 7. Specific surface area and crystallite sizes depending on the cosolvent used for the hydrolysis reaction. Synthesis conditions: c[alkoxide] = 0.17 mol·L^{-1}, T_{hydro} = 298 K, $n[(NH_4)_2CO_3]/n[M^{3+}]$ = 1, $n[H_2O]/n[M]$ = 50.

In Figure 8, the effect of the solvent composition (methanol, 1-hexanol and water) on the HTC crystallite formation and the corresponding aspect ratios of the crystallites are depicted. In principle the ternary phase diagram of methanol, 1-hexanol and water can be divided into four areas (I–IV):

I.   Classic biphasic system. HTC crystallite appearance almost independent from solvent composition. Aspect ratio $\approx$ 1

II. HTC crystallite formation is strongly dependent on the water content. With decreasing water content, an increased anisotropic character of the HTC crystallites can be observed. x[H$_2$O] = 0.45, aspect ratio $\approx$ 3; x[H$_2$O] = 0.25, aspect ratio $\approx$ 7

III. Formation of film-like HTC morphologies with a high degree of anisotropy. x[H$_2$O] = 0.05, aspect ratio $\approx$ 25

IV. Formation of gel-like structures, which cannot be assigned as HTC structures according to the characteristic [0 0 3] and [0 0 6] reflexes.
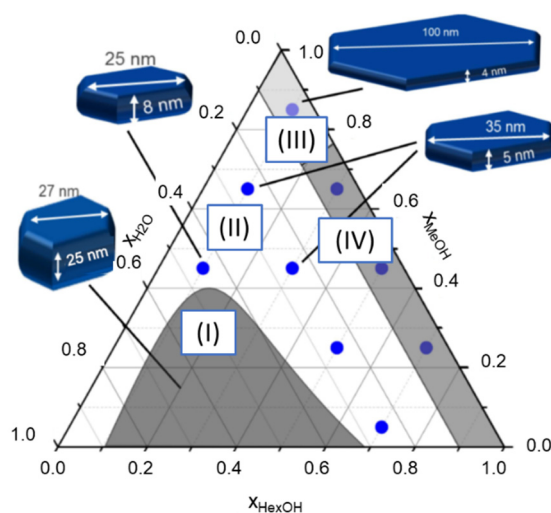
Figure 8. Ternary diagram of MeOH/1-HexOH/H$_2$O. The diagram can be divided into four hydrolysis areas using HTC synthesis strategy B. Crystallite size along the c-axis determined by X-ray diffraction programs. Crystallite size along the a- or b-axis determined by evaluating the microscopy images of the samples.

Whereas in the classical 2-phase system, the crystallite size and shape are almost independent of the solvent composition, there is clearly an influence of the solvent composition for the monophasic regime. This finding is plausible since in the biphasic system, the

hydrolysis reaction is mainly limited by the mass transport between the aqueous and the organic phase and therefore not greatly affected by the solvent composition. In the biphasic regime the formation of the biggest crystallites can be observed with an aspect ratio $d_{a,b}/d_c$ of about 1.

In the monophasic region within area II, there is no mass transport limitation coming into play, which causes the HTC crystallite formation to be strongly dependent on the water content. Whereas with a water content of $x[H_2O] = 0.45$ the calculated aspect ratio is about 3, at lower water concentrations of $x[H_2O] = 0.25$ the aspect ratio is already increased to 7. Despite this strong influence of the water content, the 1-hexanol/methanol ratio does not have an impact on the aspect ratio of the crystallites in this case.

Within the areas III and IV in the ternary phase diagram, at very low water contents ($x[H_2O] = 0.05$), a limitation of the HTC crystallite growth, due to the lack of water, can be witnessed. Whereas in the case of area III, film-like HTC structures are formed with a high degree of anisotropy (aspect ratio ≈ 25), in area IV, the formation of a gel without crystallinity can be observed. The different HTC formation behaviors in the areas III and IV in the ternary phase diagram can probably be attributed to an alteration in polarity, which directly influences the kinetics of crystallization of the system. Whereas the high methanol content in the area III causes the mixture to be very polar, area IV is far more non-polar due to the enhanced 1-hexanol content.

2.3. Hydrolysis of Metal Alkyl Carbonates for Cu/ZnO/Al₂O₃ Catalyst Synthesis

Methanol, with an annual global consumption of 53×10^6 t, is one of the most important base chemicals [50]. In industry, methanol is produced from H_2, CO and CO_2 over a $Cu/ZnO/Al_2O_3$ catalyst at 5–10 MPa and 493–503 K [51]. The reaction mechanism of industrial methanol synthesis on Cu/ZnO-based catalysts has been under-investigated and is still a controversial topic. In this context, a combined experimental and theoretical study showed that the active sites consist of Cu steps decorated with Zn atoms, which are stabilized by bulk defect [52]. However, it was also found that the $Cu/ZnO/Al_2O_3$ catalyst is a dynamic system with a continuously changing structure [53]. Mechanistically, it was also found that both CO and CO_2 hydrogenation pathways are active for methanol synthesis [54,55]. Copper-based catalysts for the methanol synthesis are usually obtained from co-precipitation reactions of metal nitrates [56–58]. Due to the exothermic reaction, large limits with regard to equilibrium yield and the resulting high demands due to low temperature activity, already small improvements of the catalyst activity and stability have a large impact on the process.

In the context of $Cu/ZnO/Al_2O_3$ catalysts for methanol synthesis, we utilized alkoxide precursors and solubilized them via CO_2 insertion to form metal alkyl carbonates (see Section 2.1). Subsequently, the metal alkyl carbonates were hydrolyzed with 600 equivalents of water to obtain the oxidic material, which was then calcined under synthetic air. This approach is beneficial since on the one hand the nucleation can be decoupled from growth processes, and on the other hand the absence of any foreign cations, such as Na^+ and NO_3^- as used in conventional precipitation processes, opens the potential of a simplified synthesis scheme.

(a)   Cu/Zn-based complex carbonates

For the synthesis of alkoxide-based precursors for the methanol synthesis, $Cu(O^iPr)_2$ and $Zn(O^iPr)_2$ were treated with 2-(2-methoxyethoxy) ethanol. Afterwards $Al(OMEE)_3$ was added and the mixture was reacted with gaseous CO_2 (see Section 2.1). The resulting solution was then hydrolyzed and washed with water. Hereby, a clear dependency of the phase formation of the water equivalents used during the hydrolysis became obvious (Figure 9). Whereas small amounts of water ($h_{equ} = 2.5$ or 20) led to the formation of amorphous materials, the addition of larger amounts of water caused crystalline hydrotalcite-like compounds and zinc malachite to form ($h_{equ} = 200$ or 600). Consequently, the material, hydrolyzed with 600 equivalents of water, was applied as a catalyst for the methanol synthesis.
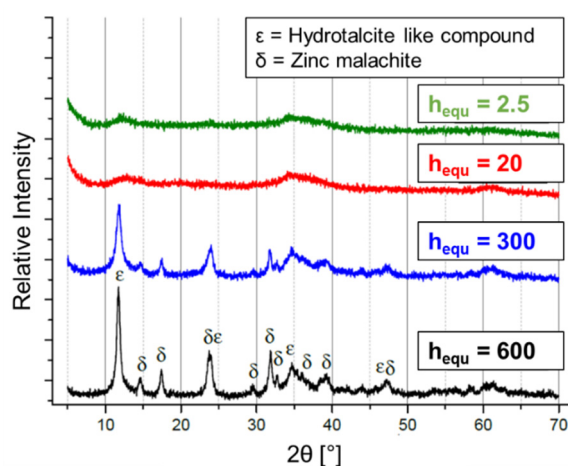
Figure 9. PXRD patterns of the dried catalyst precursors depending on the hydrolysis equivalents added (h_{equ}). Catalyst system: $Cu_{0.61}Zn_{0.21}Al_{0.18}$.

After the hydrolysis, the resulting materials were calcined under synthetic air and a solid of the composition $Cu_{0.61}Zn_{0.21}Al_{0.18}$ was obtained. The appearance of CuO, ZnO and $ZnAl_2O_4$ only occurs at calcination temperatures above 873 K (Figure 10). Very similar observations with respect to the thermal treatment were made by Behrens et al., for CuZnAl hydrotalcite-like precursors with Al contents between 30 and 40% [59].
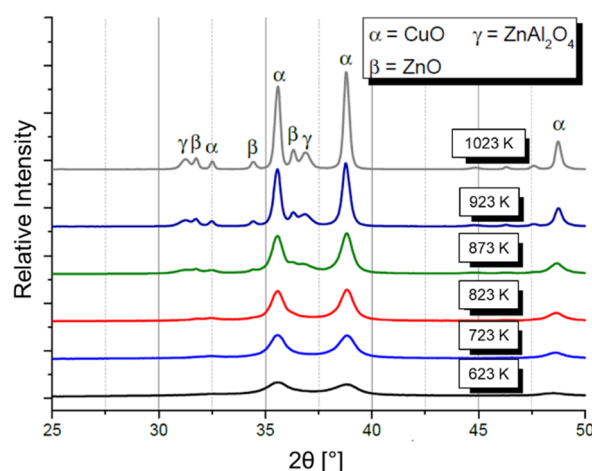
Figure 10. PXRD patterns of the dried catalyst precursors, hydrolyzed using 600 equivalents of water, depending on the calcination temperature. T_{calc} = 2 h, heating rate = 1 K·min^{-1}. Catalyst system: $Cu_{0.61}Zn_{0.21}Al_{0.18}$.

Further to this, the influence of the calcination time and temperature on the methanol space time yield (STY) was investigated. The calcination of the samples was carried out at a temperature in the range of 723–973 K (723, 823, 873, 898, 928, 973 K) for 2 to 24 h. This parameter corridor was selected based on the analysis of the specific surface area of the materials depending on the calcination temperature and time (see ESI for further information). As reference catalysts, a commercially relevant sample Cu/Zn/Al (NP-Refcat-$Cu_{0.5}Zn_{0.3}Al_{0.2}$) and a low temperature sample Cu/Zn/Al (HP-Refcat-$Cu_{0.61}Zn_{0.21}Al_{0.18}$) were utilized.

The methanol space time yield of the materials calcined at 873 K is shown in Figure 11, whereby a clear dependency on the calcination time becomes obvious. The STY can be improved when the calcination time is increased from 1 to 2 h. Afterwards a decrease in the STY with increasing holding period can be witnessed. With a holding period of 2 h, STYs comparable to the commercial MeOH catalyst (NP-Refcat) could be reached. When other

calcination temperatures and holding times were selected, the MeOH STY of the reference catalysts could not be reached (see ESI for further information).
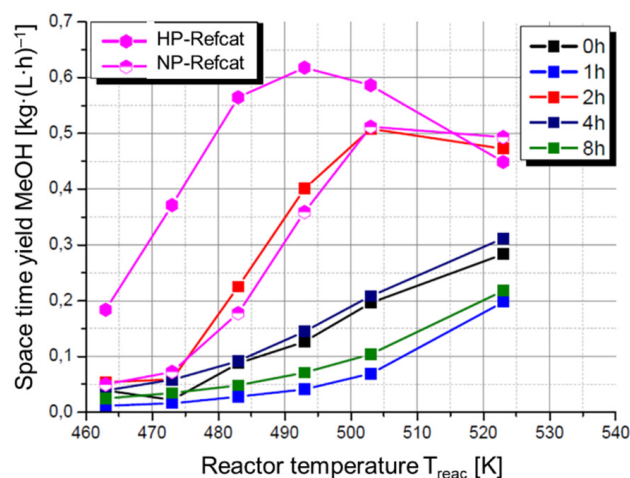
Figure 11. MeOH space time yield depending on the reactor temperature and the duration of the calcination. Catalyst system: $Cu_{0.61}Zn_{0.21}Al_{0.18}$, h_{equ} = 600, T_{calc} = 873 K. Catalytic tests: *p* = 5 MPa, GHSV = 2400 h^{-1}, S = 2, Feed = 22 vol% H_2, 62 vol% CO, 6 vol% CO_2, 10 vol% Ar.

When the gas hourly space velocity is increased from 2400 h^{-1} to 4000 h^{-1}, a similar trend is observed (Figure 12). Whereas the samples, calcined for 0 or 1 h, show an almost identical MeOH STY, a holding period of 2 h leads to a clear enhancement of the STY, which is only 15% under the performance of the commercial MeOH catalyst (NP-Refcat). As seen before, a further increase in the calcination time caused the MeOH STY to drop drastically.
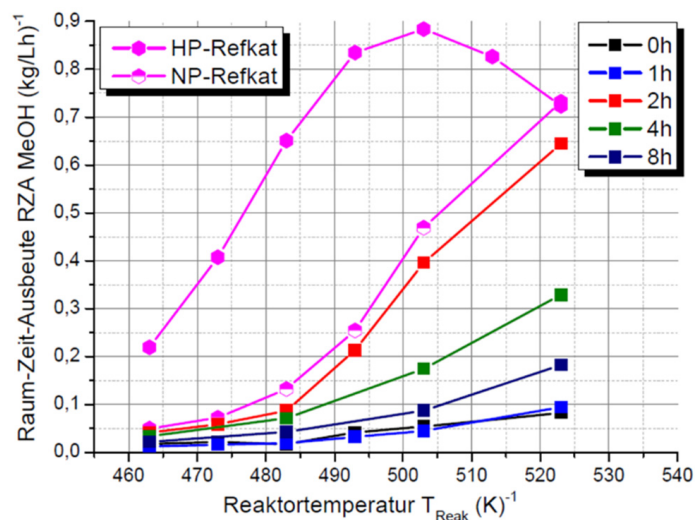
Figure 12. Space time yield MeOH depending on the reactor temperature and the duration of the calcination. Catalyst system: $Cu_{0.61}Zn_{0.21}Al_{0.18}$, h_{equ} = 600 T_{calc} = 873 K. Catalytic tests: *p* = 5 MPa, GHSV = 4000 h^{-1}, S = 2, Feed = 22 vol% H_2, 62 vol% CO, 6 vol% CO_2, 10 vol% Ar.

To explore the dependency of the MeOH STY on the calcination time, the materials calcined at 873 K for 0 to 8 h were analyzed by PXRD (Figure 13). From the decrease in the half width of the CuO reflexes, it becomes obvious that an enhanced calcination time influences the grain growth of CuO. Simultaneously, the ZnO and $ZnAl_2O_4$ reflexes become more pronounced, pointing towards the decomposition of the ht-carbonate [59].
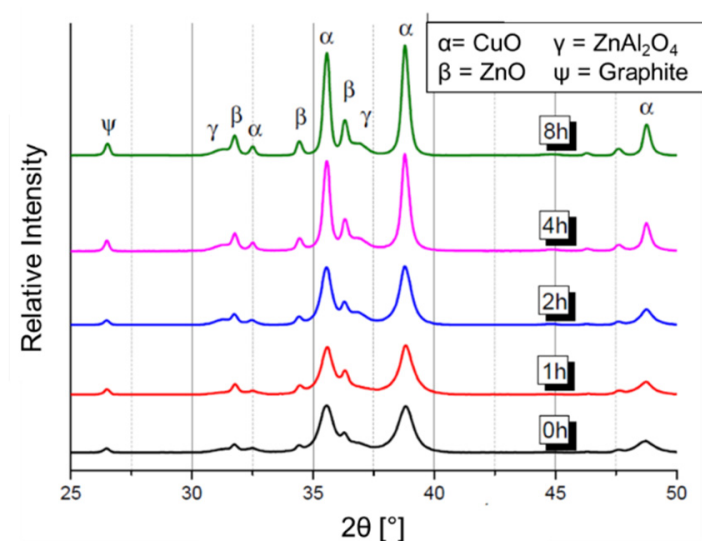
Figure 13. PXRD patterns depending on the duration of the calcination. Catalyst system: $Cu_{0.61}Zn_{0.21}Al_{0.18}$, h_{equ} = 600, T_{calc} = 823 K, heating rate = 1 K·min^{-1}.

Based on the diffractograms shown in Figure 13, the crystallite copper oxide crystallite sizes were calculated (Figure 14). An almost linear increase in the CuO crystallite sizes with enhanced calcination time can be observed. Therefore, the calcination temperature and the time influence the thermally induced conversion processes within the catalyst.
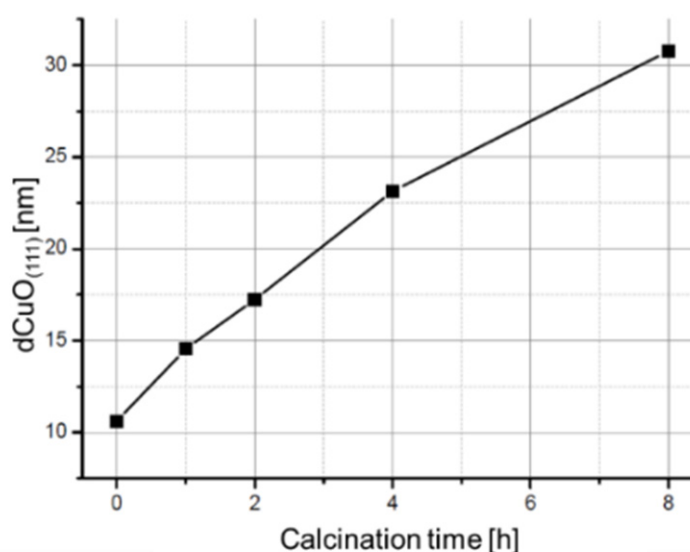
Figure 14. Calculated crystallite size dCuO (111) depending on the calcination time at a calcination temperature. Catalyst system: $Cu_{0.61}Zn_{0.21}Al_{0.18}$, h_{equ} = 600, T_{calc} = 823 K, heating rate = 1 K·min^{-1}.

To rationalize the influence of the calcination temperature and duration on the methanol space time yield, the CuO crystallite sizes before and after the catalytic reaction as well as the specific surface area after the catalytic testing were analyzed (Figure 15). Although there is a clear increase in the calculated copper crystallite sizes before and after the catalytic reaction with increasing calcination temperature and time, there is no clear correlation with the observed methanol space time yield. A similar conclusion can be drawn from the specific surface area. Again, the increase in calcination temperature has a direct influence on the specific surface area; however, no correlation with the MeOH STY can be made.
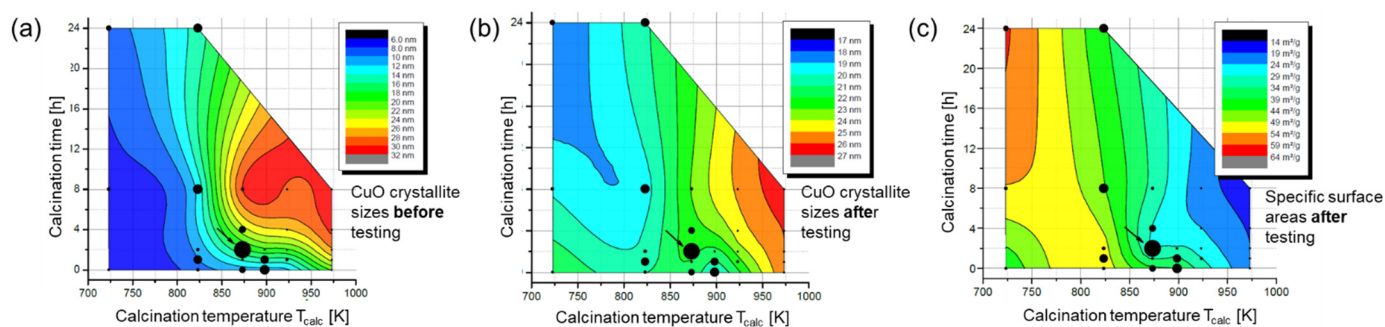
Figure 15. Contour plots of the (**a**) calculated CuO crystallite sizes before and (**b**) after the catalytic testing as well as (**c**) the specific surface area after catalytic testing depending on the calcination temperature and time. The normalized MeOH STYs are depicted as black circles. Normalization was carried out with respect to the highest MeOH STY reached (demonstrated by the black arrow) using a calcination temperature of 873 K and a holding time of 2 h. Catalyst system: $Cu_{0.61}Zn_{0.21}Al_{0.18}$, $h_{equ.}$ = 600. Catalytic tests: p = 5 MPa, GHSV = 24,000 h^{-1}, T_{react} = 503 K, S = 2, Feed = 22 vol% H_2, 62 vol% CO, 6 vol% CO_2, 10 vol% Ar.

Although it was empirically found that the calcination temperature and time has a direct influence on the catalytic performance of the $Cu/ZnO/Al_2O_3$ catalysts, no clear correlations with other structural parameters, such as the copper oxide crystallite sizes or the specific surface areas, was observed. This points towards a complex interplay of different structural and electronical factors. The complexity of the structural parameters that influence the catalytic activity under industrially relevant conditions and the fact that only a small and varying fraction of the metallic Cu surface is catalytically active has already been described by Schlögl and co-workers [52]. These findings demonstrate the need for a very detailed parameter study, which can definitely be supported by high throughput technology, [60–62] to find and optimize suitable materials for heterogeneous catalysis.

(b) Zr-promoted $Cu/ZnO/Al_2O_3$ catalysts

The use of zirconium for the synthesis of MeOH catalysts is described extensively in the literature [63–71]. In copper-based methanol catalysts, zirconium is most likely to act as chemical and structural promoter. Certain authors argue that migration of zirconium cations into the metallic copper leads to an increased formation of Cu^+ species [64,69] and therefore an enhanced catalytic activity. In terms of structural promotion, zirconium tends to lead to an enhanced specific surface area [66,69,72] and copper dispersion (and higher specific Cu surface area) [69,72,73] as well as smaller copper crystallites [69] after reduction.

Zirconium-promoted catalysts were obtained from the reaction of $Cu(O^iPr)_2$ and $Zn(O^iPr)_2$ in 2-(2-methoxyethoxy) ethanol. Subsequently, $Al(OMEE)_3$ and $Zr(OMEE)_4$ were added and the mixture was treated with CO_2. Afterwards the hydrolysis was carried out with 600 equivalents of water and a blue green solid was obtained, which was found to consist of $Cu_{0.61}Zn_{0.21}Al_{0.18-(0.18·xZr)}Zr_{(0.18·xZr)}$ after washing with water and drying. Based on the results shown before for the unpromoted $Cu/ZnO/Al_2O_3$ materials, the samples were calcined at 873 K for 2 h (see ESI for further information) and the zirconium-promoted materials were tested as catalysts in the synthesis of methanol from H_2, CO and CO_2. From Figure 16, it becomes obvious that the zirconium amount has an enormous influence on the methanol space time yield at a GHSV of 2400 h^{-1}. When 40% of the aluminum in the materials is displaced by zirconium, higher space time yields than the commercial reference MeOH catalyst (NP-Refcat) can be achieved. However, a larger amount of zirconium leads only to a minor performance enhancement. At a reactor temperature of 493 K the MeOH STY is only 20% lower than the STY obtained with the commercial low temperature reference MeOH catalyst (HP Refcat).
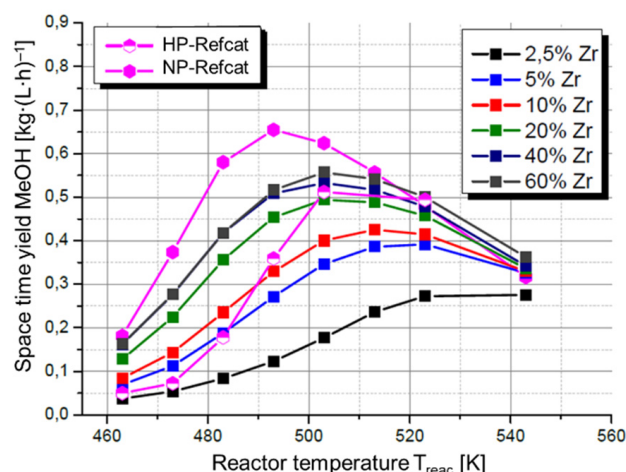
Figure 16. Space time yield MeOH depending on the reactor temperature and the zirconium substituted amount of Al in %. Catalyst system: $Cu_{0.61}Zn_{0.21}Al_{0.18-(0.18\cdot xZr)}Zr_{(0.18\cdot xZr)}$, h_{equ} = 600, T_{calc} = 873 K, t_{calc} = 2 h. Catalytic tests: p = 5 MPa, GHSV = 2400 h^{-1}, S = 2, Feed = 22 vol% H_2, 62 vol% CO, 6 vol% CO_2, 10 vol% Ar.

To investigate the influence of the Zr promoter amount further, the CuO crystallite sizes were calculated from the CuO (111) reflexes before and after the catalytic testing (Figure 17). With an increasing degree of substitution, the CuO crystallite sizes before and after the testing decrease. After the catalytic testing, the CuO crystallites are about 50% smaller when going from X_{Zr} = 2.5% to X_{Zr} = 60%.
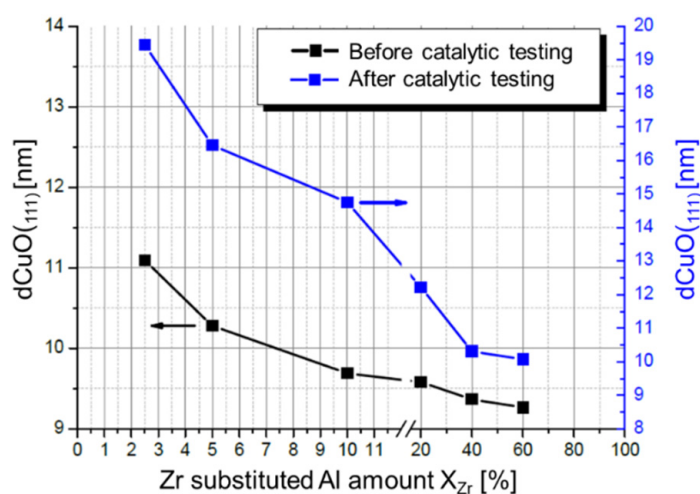
Figure 17. Calculated CuO crystallite size before and after the catalytic test depending on the amount of zirconium substituting Al. Catalyst system: $Cu_{0.61}Zn_{0.21}Al_{0.18-(0.18\cdot xZr)}Zr_{(0.18\cdot xZr)}$, h_{equ} = 600, T_{calc} = 873 K, t_{calc} = 2 h, heating rate = 1 $K\cdot min^{-1}$.

To explore the role of Zr as structural promoter in the $Cu/ZnO/Al_2O_3$ system, the specific surface areas of the materials were determined before and after the catalytic testing depending on the degree of Zr substitution (Figure 18). Hereby, it becomes obvious that an increase in the degree of substitution to 20% leads to an enhanced specific surface area. Above X_{Zr} = 20% leads to a reduction in the specific surface area. However, even at X_{Zr} = 60%, the specific surface area is larger than for the ones observed for very low degrees of substitution. This trend is observed for the materials before and after the catalytic tests. Overall, it can be said that Zr acts as a structural promoter and leads to an enhanced Cu crystallite size and an increased specific surface area.
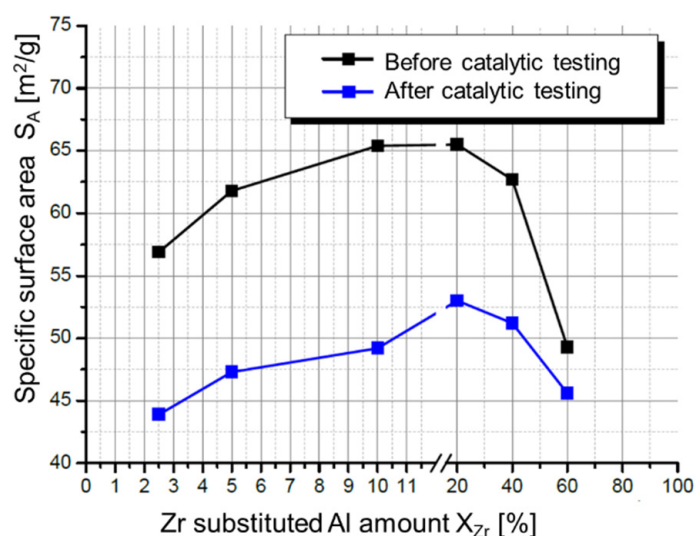
Figure 18. Specific surface areas before and after the catalytic testing depending on the amount of zirconium substituting Al. Catalyst system: $Cu_{0.61}Zn_{0.21}Al_{0.18-(0.18\cdot xZr)}Zr_{(0.18\cdot xZr)}$, h_{equ} = 600, T_{calc} = 873 K, t_{calc} = 2 h, heating rate =1 K·min^{-1}.

3. Materials and Methods

3.1. Analytical Methods

Powder X-ray diffraction

For the measurement of powder diffractograms, an AXS D8 Discover/GADDS (General Area Detector Diffraction System, Bruker Corporation, Billerica, MA, USA) with HI-STAR area detector and a Bruker D8 Advance diffractometer with Lynxeye XE Detector, both with Bragg–Brentano geometry, were utilized. Both diffractometers were equipped with a Cu Kα radiation source with a wavelength of 1.540598 nm. The determination of the crystallite sizes was carried out according to the Scherrer equation, based on the full half-widths $\Delta(2\theta)$ obtained from the diffractograms, and the Scherrer form factor K = 0.9.

$$\Delta(2\theta) = \frac{K \cdot \lambda}{L \cdot \cos(\theta_0)} \tag{1}$$

N$_2$ physisorption

The specific surface areas were determined via N$_2$ physisorption measurements using a Micromeritics TriStar II 3020. Before the actual measurements, the samples were preconditioned at 423 K for 60 min under vacuum. Afterwards the samples were cooled to 77 K and the adsorption isotherms were recorded. The analyses of the isotherms were carried out according to the Brunauer, Emmett und Teller BET-method [74].

ATR-IR spectroscopy

ATR-IR spectroscopic measurements were carried out using an ALPHA-T FT-IR spectrometer with a diamond ATR unit from Bruker (Bruker Corporation, Billerica, MA, USA). To avoid any hydrolysis of metal alkoxides, the sample preparation was carried out in a glovebox under argon atmosphere.

3.2. Experimental Details

In the following section exemplary examples of the synthesis of different alkoxide precursors, HTCs and bulk catalysts are given. Granular lithium, Al(O^{i}Pr)$_3$, Ti(O^{n}Pr)$_4$ and Mg(OEt)$_2$ were purchased from Sigma Aldrich (Sigma Aldrich Corporation, St. Louis, MO, USA), whereas CuCl$_2$, ZnCl$_2$, CoCl$_2$, MnCl$_2$, Zr(O^{n}Pr)$_4$ were obtained from Alfa Aesar (Haverhill, MA, USA).

Preparation of Cu(O^{i}Pr)$_2$

In total 3.82 g (0.55 mol) elemental lithium in granular form was reacted slowly with 750 g *iso*-propanol at 80 °C. After no elemental lithium was visible anymore, the mixture was added to a homogeneous dark green solution of 36.98 g (0.275 mol) anhydrous CuCl$_2$ in 830 g anhydrous *iso*-propanol, which was heated before at 70 °C for 1 h. Immediately, Cu(O^{i}Pr)$_2$ was formed as dark green solid and the viscosity of the mixture strongly increased. Subsequently, the mixture was stirred at 68 °C for 1 h and afterwards cooled to room temperature with an ice bath. The copper(II) alkoxide was isolated via centrifugation, washing with *iso*-propanol and drying. The yield typically amounts 85–93%.

Preparation of Zn(O^{i}Pr)$_2$

In total, 5.30 g (0.76 mol) elemental lithium was reacted slowly with 940 g *iso*-propanol at 80 °C. As soon as the reaction was completed, the lithium *iso*-propoxide solution was reacted with a pale yellow Zn(O^{i}Pr)$_2$ solution, which was synthesized before from 52.04 g (0.38 mol) ZnCl$_2$ and anhydrous *iso*-propanol (780 g) at 50 °C for 1 h. Immediately after the addition, Zn(O^{i}Pr)$_2$ was formed as white solid, whereas an enhanced viscosity of the reaction mixture was observed. The mixture was stirred for another hour at 69 °C and subsequently cooled to room temperature with an ice bath. The products were obtained after centrifugation, washing with *iso*-propanol and drying under vacuum. The yield typically amounts 91–95%.

Preparation of Co(O^{i}Pr)$_3$

In total, 17.95 g (0.14 mol) anhydrous CoCl$_2$ was reacted with anhydrous *iso*-propanol. After the mixture was heated to 50 °C for 1 h, a dark purple solution was obtained. This solution was added to a ^{i}PrOH solution of 1.92 g (0.28 mol) lithium, which was stepwise reacted with 315 g *iso*-propanol at 80 °C. Immediately after the addition, Co(O^{i}Pr)$_2$ was formed as dark purple solid and, simultaneously, the viscosity of the mixture was increased. This mixture was stirred at 69 °C for 1 h and then cooled down with an ice bath. The product was isolated via centrifugation followed by washing and drying under vacuum. Typically, yields of 94% can be achieved.

Preparation of Mn(OMe)$_2$

In total, 27.20 g (0.22 mol) anhydrous MnCl$_2$ was reacted with 280 g dry methanol. The mixture was heated to 50 °C for 1 h and a pale pink solution was obtained. This solution was then added to a before prepared methanolic lithium solution (obtained from 3.0 g (0.43 mol) lithium in methanol at 80 °C), whereby a pale pink solid was formed. Simultaneously the viscosity of the mixture was increased. The mixture was heated at 69 °C for 1 h and subsequently cooled down with an ice bath. The product was isolated by centrifugation, washing with methanol and drying under vacuum. Typical yields of 82% can be achieved.

Preparation of Al(OMEE)$_3$

In total, 100 g (0.49 mol) Al(O^{i}Pr)$_3$ was suspended in 176.5 g (1.47 mol) of liquid 2-(2-methoxyethoxy) ethanol. After stepwise heating of the suspension to 180 °C, a homogenous solution was formed and, simultaneously, *iso*-propanol was generated, which was removed from the mixture via distillation. Yields of 98% can be achieved.

Preparation of Zr(OMEE)$_4$

In total, 165 g of a 70 wt% solution of Zr(O^{n}Pr)$_4$ in *n*-propanol was mixed with 169.4 g (1.41 mol) of liquid 2-(2-methoxyethoxy) ethanol. The mixture was heated stepwise to 180 °C under formation of *n*-propanol, which was removed via distillation. Yields of 94% can be achieved.

General preparation of hydrotalcites

To a mixture of 3.1 g (0.03 mol) Mg(OEt)$_2$ and 1.85 g (0.10 mol) Al(O^{i}Pr)$_3$, 9.2 g (0.09 mol) 1-hexanol was added. After the removal of ethanol and *iso*-propanol via distillation at 393 K, Mg$_{0.75}$Al$_{0.25}$-hexanolate was obtained. Depending on the composition of the hydrolysis mixture, further 1-hexanol was added. The hexanolate was added to a mixture of methanol, water and ammonium carbonate under stirring. The resulting precipitate was filtered off after 24 h, washed twice with 50 g acetone and three times with 150 g water. Subsequently, the precipitate was dried at 80 °C for 16 h.

Preparation of Mg$_6$Al$_2$(OH)$_{18}$·4 H$_2$O

In total, 12.43 g (0.11 mol) magnesium ethoxide and 7.40 g (0.04 mol) aluminum *iso*-propoxide were filled into a 500 mL reaction vessel under inert gas atmosphere. Subsequently, 66 mL of 1-hexanol was added. Ethanol was distilled off at 80 °C and the *iso*-propanol was distilled off at 84 °C. The resulting metal hexanolate solution was heated at 80 °C for 1 h under stirring. Then 65 mL methanol was added. To trigger the hydrolysis, 31 mL of an aqueous solution of 3.48 g ammonium carbonate was added to the metal hexanolate solution under vigorous stirring, while the temperature of the hexanolate solution was kept at 80 °C After the addition of the aqueous carbonate solution, the heating of the mixture (at 80 °C), as well as stirring of the mixture, was continued for 5 h to equilibrate and to age the precipitate. Afterwards the precipitate was filtered off and subjected to a washing process, which consisted of a first washing step with acetone and a second washing step with water. In the next step the precipitate was placed into a drying oven for 12 h at 80 °C. The yield of dried product corresponded to 98 wt% of the theoretical yield.

Preparation of Mg$_6$Al$_2$(CO$_3$)(OH)$_{16}$·4 H$_2$O

In total, 12.43 g (0.11 mol) magnesium ethoxide and 7.40 g (0.04 mol) aluminum *iso*-propoxide were filled into a 500 mL reaction vessel under inert gas atmosphere. Then, 18.4 mL dry 1-hexanol were added to the metal salts. The metal salts were converted into the metal hexanolates by exchanging the alcohol groups and removal of the low boiling alcohols via distillation, whereby ethanol was distilled off at 80 °C and *iso*-propanol distilled off at 84 °C. In a subsequent step the metal hexanolate was converted into the metal hexyl carbonate solution by treating the solution with gaseous CO$_2$. The CO$_2$ was delivered to the solution by bubbling gaseous CO$_2$ (with a tube equipped with a jet nuzzle) into the solution for one hour while the solution was heated at 80 °C. The flow rate of the CO$_2$ supply was 1000 mL per minute. The yield of the resulting solution containing metal hexyl carbonate was 98% of the theoretical yield. Then the metal carbonate hexanolate solution was heated at 80 °C for 1 h under agitation. In the next step, 65 mL of methanol was added to the solution. This step was followed by the hydrolysis step, which was performed by the addition of 31 mL H$_2$O under vigorous stirring. The stirring of the mixture was continued for a period of 5 h. The resulting precipitate was separated from the liquid by filtration and subjected to a washing process. Washing included washing treatment with acetone and washing treatment with water. The washed precipitate was dried for 12 h at 80 °C within a drying oven. The yield of dried product was 98 wt% of the theoretical yield.

Preparation of Cu/ZnO/Al$_2$O$_3$ bulk catalysts

In total, 6.65 g (0.04 mol) Cu(O^{i}Pr)$_2$ and 2.31 g (0.01 mol) Zn(O^{i}Pr)$_2$ were treated with 160 g of 2-(2-methoxyethoxy) ethanol. After 30 min at 80 °C, a homogenous dark blue solution was formed. To this solution 4.15 g (0.01 mol) Al(OMEE)$_3$ was added and gaseous CO$_2$ (1 L·min^{-1}) was bubbled through the mixture for 1 h. The alkoxide solution was then transferred to water (1413 g, 78.48 mol, 600 equivalents). A blue green solid was formed, which was washed with 100 g of water and dried at 80 °C for 16 h. After drying, a blue green solid of the composition Cu$_{0.61}$Zn$_{0.21}$Al$_{0.18}$ was obtained. The materials were calcined under synthetic air (further information about the temperature and the time are given in the main text).

Preparation of zirconium-promoted Cu/ZnO/Al$_2$O$_3$ bulk catalysts

In total, 6.65 g (0.04 mol) Cu(O^{i}Pr)$_2$ and 2.31 g (0.01 mol) Zn(O^{i}Pr)$_2$ were treated with 160 g of 2-(2-methoxyethoxy) ethanol. The mixture was heated to 80 °C and resulted in a dark blue solution after 30 min. Subsequently, 1.66 g (0.004 mol) Al(OMEE)$_3$ and 3.68 g (0.006 mol) Zr(OMEE)$_4$ were added and gaseous CO$_2$ (1 L·min^{-1}) was bubbled through the mixture for 1 h. For the hydrolysis, the mixture was added to 1483 g (82.37 mol, 600 equivalents) of water. A blue green solid was formed, which was washed with 100 g of water and dried at 80 °C for 16 h. After drying, a blue green solid of the composition Cu$_{0.61}$Zn$_{0.21}$Al$_{0.072}$Zr$_{0.108}$ was obtained. The materials were calcined under synthetic air (further information about the temperature and the time are given in the main text).

3.3. Catalytic Testing

For the catalytic testing of the materials in the gas phase, a high throughput reactor system with 16 reactors was utilized (Figure 19). The catalytic bulk materials were mixed with corundum in a 1:1 volumetric ratio to ensure an efficient heat transfer and avoid local overheating of the catalyst and filled into the reactor with a layer of Alodur Korund WSK F100 at the bottom and at the top of the reactor. The different feed gases were added via different mass flow controllers. Gaseous samples of the reaction were taken via a multiport valve at the end of the reactor and the products were analyzed using gas chromatography (Agilent 6890). For the analysis of the permanent gases and CO$_2$, a thermal conductivity detector with a molecular sieve 5 Å-column (50 m × 0.53 mm × 50 μm) was utilized. For the analysis of organic components, a flame ionization detector with a DB1-column (60 m × 0.32 mm × 3 μm) was used.
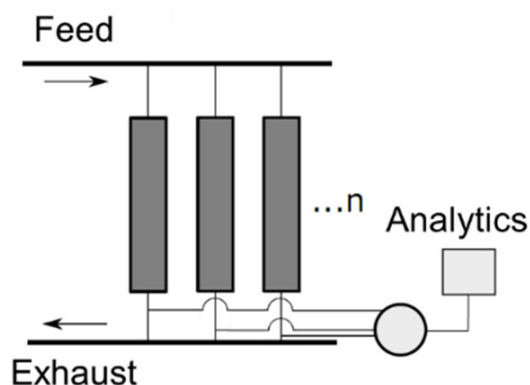
Figure 19. Schematic representation of a high throughput reactor system with online analytical methods. The sampling is carried out via multiport valves at the reactor outlet.

4. Conclusions

Metal alkoxides were solubilized using different strategies, such as derivatization, hetero-metallization or/and CO$_2$ insertion. Through the reaction of metal alkoxides with carbon dioxide, access to soluble metal alkyl carbonates could be granted via CO$_2$ insertion into the metal–oxygen bond of the alkoxide. This CO$_2$ insertion strategy is therefore not only an alternative solubilization approach but also provides access to phase-pure, well-characterized metal alkyl carbonates, which can be applied in controlled hydrolysis and condensation processes for sol–gel syntheses as a way to access relevant inorganic functional materials, such as LDHs and mixed metal oxides. Further kinetic studies of the CO$_2$ insertion into metal alkoxides are currently under investigation.

To prevent the precipitation in biphasic systems (aqueous/organic) and, inherently, not to compromise regarding mass transport limitations between the two phases during the hydrolysis of the metal alkoxide precursor, the application of a cosolvent was investigated. Overall, the application of a cosolvent influences the specific surface area, the size and the morphology of the final materials. It is worth mentioning that the solvents used in this

work were antisolvents for the final product (LDHs). This in turn allowed us to synthesize the ultra-thinnest LDH materials.

The application potential of the metal alkyl carbonates as catalyst precursors was demonstrated in the synthesis of methanol from CO, CO_2 and H_2. Therefore, the CO_2-inserted alkoxide precursors were hydrolyzed to obtain $Cu/ZnO/Al_2O_3$ and Zr-promoted $Cu/ZnO/Al_2O_3$ bulk catalysts. The calcination time and duration of the precursor affects the catalytic performance of the resulting materials in the direct synthesis of methanol. The reached STY is only 15% below a commercial reference methanol catalyst, and by using zirconia as promoter, the MeOH STY could even be increased further with the $Cu_{0.61}Zn_{0.21}Al_{0.072}Zr_{0.108}$ system. This STY is about 10% higher than the one obtained with a commercial reference MeOH catalyst and only 15% below a commercial low temperature MeOH catalyst.

5. Patents

Schunk, S.A.; Lizandara-Pueyo, C.; Futter, C.; Emmert, T.P. Process for the Preparation of Oxide Materials, Layered Double Hydroxide Materials, Hydroxide Materials and Carbonate-Based Materials. WO 2016/096990 A1, 23 June 2016.

Schunk, S.A.; Lizandara-Pueyo, C.; Jevtovikj, J.; Emmert, T.; Lejkowski, M.; Müller, R. Process for the Preparation of Carbonate Containing Metal Oxides-Hydroxides by Employing Metal Alkoxide Solutions Containing Metal Alkyl Carbonate Groups. EP 3 192 772 A1, 15 January 2016.

Supplementary Materials: Supporting information, such as additional information about the solubilization strategies, the access to layered double hydroxide-carbonates through hydrolysis of metal alkoxide-CO_2-complexes and the synthesis of $Cu/ZnO/Al_2O_3$ catalysts can be downloaded at: https://www.mdpi.com/article/10.3390/catal12050554/s1.

Author Contributions: Conceptualization: S.H., C.L.-P. and S.A.S.; methodology: T.P.E. and I.J., writing—original draft preparation: S.H.; writing—review and editing, C.L.-P., S.A.S. and R.G. All authors have read and agreed to the published version of the manuscript.

Funding: We gratefully acknowledge funding by BASF SE and hte GmbH.

Data Availability Statement: Data are made available two extended sources: (I) reference [8] (II) patent publications mentioned under Section 5.

Acknowledgments: We gratefully acknowledge support from BASF SE and hte GmbH.

Conflicts of Interest: The authors declare no conflict of interest.

References

1. Lu, H.; Wright, D.S.; Pike, S.D. The use of mixed-metal single source precursors for the synthesis of complex metal oxides. *Chem. Commun.* **2020**, *56*, 854–871. [CrossRef] [PubMed]
2. Hanf, S.; Matthews, P.D.; Li, N.; Luo, H.K.; Wright, D.S. The Influence of Halides in Polyoxotitanate Cages; Dipole Moment, Splitting and Expansion of d-Orbitals and Electron-Electron Repulsion. *Dalt. Trans.* **2017**, *46*, 578–585. [CrossRef] [PubMed]
3. Tatte, T.; Hussainov, M.; Paalo, M.; Part, M.; Talviste, R.; Kiisk, V.; Mändar, H.; Põhako, K.; Pehk, T.; Reivelt, K.; et al. Alkoxide-based precursors for direct drawing of metal oxide micro- and nanofibres. *Sci. Technol. Adv. Mater.* **2011**, *12*, 34412. [CrossRef] [PubMed]
4. Kessler, V.G. The Synthesis and Solution Stability of Alkoxide Precursors. In *Handbook of Sol-Gel Science and Technology: Processing, Characterization and Applications*; Springer International Publishing: Berlin/Heidelberg, Germany, 2018; pp. 31–80.
5. Turova, N.Y.; Turevskaya, E.P.; Kessler, V.G.; Yanovskaya, M.I. *The Chemistry of Metal Alkoxides*; Kluwer Academic Publishers Group: Drive Norwell, MA, USA, 2002.
6. Turevskaya, E.P.; Yanovskaya, M.I.; Turova, N.Y. Preparation of Oxide Materials from Metal Alkoxides. In *Inorganic Materials*; Springer: Berlin/Heidelberg, Germany, 2000; pp. 260–270.
7. Mishra, S.; Daniele, S. Molecular Engineering of Metal Alkoxides for Solution Phase Synthesis of High-Tech Metal Oxide Nanomaterials. *Chem. Eur. J.* **2020**, *26*, 9292–9303. [CrossRef]
8. Emmert, T.P. Übergangsmetallalkoxide als Precursoren für nano-strukturierte Funktionsmaterialen. Ph.D. Dissertation, Leipzig University, Leipzig, Germany, 2016.

9. Saini, A.; Jat, S.K.; Shekhawat, D.S.; Kumar, A.; Dhayal, V.; Agarwal, D.C. Oxime-modified aluminium(III) alkoxides: Potential precursors for γ-alumina nano-powders and optically transparent alumina film. *Mater. Res. Bull.* **2017**, *93*, 373–380. [CrossRef]

10. Díez-Sierra, J.; López-Domínguez, P.; Rijckaert, H.; Rikel, M.; Hänisch, J.; Khan, M.Z.; Falter, M.; Bennewitz, J.; Huhtinen, H.; Schäfer, S.; et al. High Critical Current Density and Enhanced Pinning in Superconducting Films of $YBa_2Cu_3O_7$-ΔNanocomposites with Embedded $BaZrO_3$, $BaHfO_3$, $BaTiO_3$, and $SrZrO_3$Nanocrystals. *ACS Appl. Nano Mater.* **2020**, *3*, 5542–5553. [CrossRef]

11. Bäcker, M.; Bennewitz, J.; de Keukeleere, K.; de Roo, J.; van Driessche, I.; Falter, M.; Dominguez, P.L.; Meyer, A.; Rijackaert, H.; Schäfer, S.; et al. Process for Producing Nanoparticles. WO2020049019A1, 12 March 2020.

12. Brinker, C.J.; Scherer, G.W. *Sol-Gel Science: The Physics and Chemistry of Sol-Gel Processing*; Elsevier Inc.: Amsterdam, The Netherlands, 2013.

13. Danks, A.E.; Hall, S.R.; Schnepp, Z. The Evolution of "sol-Gel" Chemistry as a Technique for Materials Synthesis. *Mater. Horiz.* **2016**, *3*, 91–112. [CrossRef]

14. Clément, S.; Mehdi, A. Sol-Gel Chemistry: From Molecule to Functional Materials. *Molecules* **2020**, *25*, 2538. [CrossRef]

15. Liu, X.; Iocozzia, J.; Wang, Y.; Cui, X.; Chen, Y.; Zhao, S.; Li, Z.; Lin, Z. Noble Metal-Metal Oxide Nanohybrids with Tailored Nanostructures for Efficient Solar Energy Conversion, Photocatalysis and Environmental Remediation. *Energy Environ. Sci.* **2017**, *10*, 402–434. [CrossRef]

16. Ma, C.; Alvarado, J.; Xu, J.; Clément, R.J.; Kodur, M.; Tong, W.; Grey, C.P.; Meng, Y.S. Exploring Oxygen Activity in the High Energy P2-Type $Na_{0.78}Ni_{0.23}Mn_{0.69}O_2$ Cathode Material for Na-Ion Batteries. *J. Am. Chem. Soc.* **2017**, *139*, 4835–4845. [CrossRef]

17. Mensinger, Z.L.; Gatlin, J.T.; Meyers, S.T.; Zakharov, L.N.; Keszler, D.A.; Johnson, D.W. Synthesis of Heterometallic Group 13 Nanoclusters and Inks for Oxide Thin-Film Transistors. *Angew. Chem. Int. Ed.* **2008**, *47*, 9484–9486. [CrossRef] [PubMed]

18. Dubal, D.P.; Gomez-Romero, P. (Eds.) *Metal Oxides in Supercapacitors*, 1st ed.; Elsevier: Amsterdam, The Netherlands, 2017.

19. Li, W.M.; Zhao, J.F.; Cao, L.P.; Hu, Z.; Huang, Q.Z.; Wang, X.C.; Liu, Y.; Zhao, G.Q.; Zhang, J.; Liu, Q.Q.; et al. Superconductivity in a unique type of copper oxide. *Proc. Natl. Acad. Sci. USA* **2019**, *116*, 12156–12160. [CrossRef] [PubMed]

20. Mehrotra, R.C. Transition-Metal Alkoxides. *Adv. Inorg. Chem.* **1983**, *26*, 269–335. [CrossRef]

21. Bradley, D. Metal Alkoxides and Dialkylamides. *Adv. Inorg. Chem.* **1972**, *15*, 259–322. [CrossRef]

22. Bradley, D.C.; Mehrotra, R.C.; Wardlaw, W. Structural chemistry of the alkoxides. Part I. Amyloxides of silicon, titanium, and zirconium. *J. Chem. Soc.* **1952**, 2027–2032. [CrossRef]

23. Bradley, D.C.; Mehrotra, R.C.; Wardlaw, W. Structural chemistry of the alkoxides. Part II. Tertiary alkoxides of silicon, titanium, zirconium, and hafnium. *J. Chem. Soc.* **1952**, 4204–4209. [CrossRef]

24. Bradley, D.C.; Mehrotra, R.C.; Wardlaw, W. Structural chemistry of the alkoxides. Part III. Secondary alkoxides of silicon, titanium, and zirconium. *J. Chem. Soc.* **1952**, 5020–5023. [CrossRef]

25. Bradley, D.C.; Mehrotra, R.C.; Swanwick, J.D.; Wardlaw, W. 412. Structural chemistry of the alkoxides. Part IV. Normal alkoxides of silicon, titanium, and zirconium. *J. Chem. Soc.* **1953**, 2025–2030. [CrossRef]

26. Daniele, S.; Tcheboukov, D.; Pfalzgraf, L.G.H. Functional homo- and heterometallic alkoxides as precursors for sol–gel routes to transparent $ZnGa_2O_4$ coatings. *J. Mater. Chem.* **2002**, *12*, 2519–2524. [CrossRef]

27. Caulton, K.G.; Pfalzgraf, L.G.H. Synthesis, Structural Principles, and Reactivity of Heterometailic Alkoxides. *Chem. Rev.* **1990**, *90*, 969–995. [CrossRef]

28. Arkled, B. (Ed.) Double Metal Alkoxides/Heterometallic Alkoxides. In *Silicon, Germanium, Tin and Lead Compounds; Metal Alkoxides, Diketonates and Carboxylates*; Gelest Inc.: Morrisville, PA, USA, 1995.

29. Livage, J.; Henry, M.; Sanchez, C. Sol-gel chemistry of transition metal oxides. *Prog. Solid State Chem.* **1988**, *18*, 259–341. [CrossRef]

30. Hazari, N.; Heimann, J.E. Carbon Dioxide Insertion into Group 9 and 10 Metal-Element σ Bonds. *Inorg. Chem.* **2017**, *56*, 13655–13678. [CrossRef] [PubMed]

31. Behrendt, W.; Gattow, G. Über Chalkogenolate. LXII. Untersuchungen Über Halbester Der Kohlensäure 2. Darstellung Und Eigenschaften Der Monomethylkohlensäure. *ZAAC* **1973**, *398*, 198–206.

32. Hidai, M.; Hikita, T.; Uchida, Y. Reactions of carbon dioixde with transition metal alkoxides. *Chem. Lett.* **1972**, *1*, 521–522. [CrossRef]

33. Chisholm, M.H.; Cotton, F.A.; Extine, M.W.; Reichert, W.W. The molybdenum-molybdenum triple bond. 4. Insertion reactions of hexakis(alkoxy)dimolybdenum compounds with carbon dioxide and single-crystal X-ray structural characterization of bis(tert-butylcarbonato)tetrakis(tert-butoxy)dimolybdenum. *J. Am. Chem. Soc.* **2002**, *100*, 1727–1734. [CrossRef]

34. Tsuda, T.; Saegusa, T. Reaction of cupric methoxide and carbon dioxide. *Inorg. Chem.* **1972**, *11*, 2561–2563. [CrossRef]

35. Chisholm, M.H.; Zhou, Z. New generation polymers: The role of metal alkoxides as catalysts in the production of polyoxygenates. *J. Mater. Chem.* **2004**, *14*, 3081–3092. [CrossRef]

36. Polarz, S.; Pueyo, C.L.; Krumm, M. The molecular path to inorganic materials—Zinc oxide and beyond. *Inorg. Chim. Acta* **2010**, *363*, 4148–4157. [CrossRef]

37. Prasad, S.; Kumar, V.; Kirubanandam, S.; Barhoum, A. Engineered Nanomaterials: Nanofabrication and Surface Functionalization. In *Emerging Applications of Nanoparticles and Architectural Nanostructures: Current Prospects and Future Trends*; Elsevier Inc.: Amsterdam, The Netherlands, 2018; pp. 305–340.

38. Neto, V.D.O.S.; Freire, T.M.; Saraiva, G.D.; Muniz, C.R.; Cunha, M.S.; Fechine, P.B.A.; Nascimento, R.F.D. Water Treatment Devices Based on Zero-Valent Metal and Metal Oxide Nanomaterials. In *Nanomaterials Applications for Environmental Matrices: Water, Soil and Air*; Elsevier: Amsterdam, The Netherlands, 2019; pp. 187–225.

39. Teixeira, G.F.; Lustosa, G.M.; Zanetti, S.M.; Zaghete, M.A. Chemical synthesis and epitaxial growth methods for the preparation of ferroelectric ceramics and thin films. In *Magnetic, Ferroelectric, and Multiferroic Metal Oxides*; Elsevier: Amsterdam, The Netherlands, 2018; pp. 121–137.

40. Abou Neel, E.A.; Salih, V.; Knowles, J.C. Phosphate-Based Glasses. In *Comprehensive Biomaterials II*; Elsevier: Amsterdam, The Netherlands, 2017; pp. 392–405.

41. Opuchovic, O.; Kareiva, A. Sol–Gel Synthesis and Characterization of Iron-Containing Garnets. In *Biocompatible Hybrid Oxide Nanoparticles for Human Health*; Elsevier: Amsterdam, The Netherlands, 2019; pp. 233–261.

42. Lu, Y.; Dong, W.; Ding, J.; Wang, W.; Wang, A. Hydroxyapatite Nanomaterials: Synthesis, Properties, and Functional Applications. In *Nanomaterials from Clay Minerals: A New Approach to Green Functional Materials*; Elsevier: Amsterdam, The Netherlands, 2019; pp. 485–536.

43. Hubert-Pfalzgraf, L.G. To What Extent Can Design of Molecular Precursors Control the Preparation of High Tech Oxides? *J. Mater. Chem.* **2004**, *14*, 3113–3123. [CrossRef]

44. Kessler, V.G. Molecular structure design and synthetic approaches to the heterometallic alkoxide complexes (soft chemistry approach to inorganic materials by the eyes of a crystallographer). *Chem. Commun.* **2003**, 1213–1222. [CrossRef]

45. Hubert-Pfalzgraf, L.G. Some trends in the design of homo- and heterometallic molecular precursors of high-tech oxides. *Inorg. Chem. Commun.* **2003**, *6*, 102–120. [CrossRef]

46. Choi, J.-C.; Sakakura, T.; Sako, T. Reaction of Dialkyltin Methoxide with Carbon Dioxide Relevant to the Mechanism of Catalytic Carbonate Synthesis. *J. Am. Chem. Soc.* **1999**, *121*, 3793–3794. [CrossRef]

47. Vaccari, A. Preparation and catalytic properties of cationic and anionic clays. *Catal. Today* **1998**, *41*, 53–71. [CrossRef]

48. Cavani, F.; Trifirò, F.; Vaccari, A. Hydrotalcite-Type Anion Clays: Preparation, Properties and Applications. *Catal. Today* **1991**, *11*, 173–301. [CrossRef]

49. Hochstetter, C. Untersuchung über die Zusammensetzung einiger Mineralien. *J. Prakt. Chem.* **1842**, *27*, 375–378. [CrossRef]

50. Bertau, M.; Offermanns, H.; Plass, L.; Schmidt, F.; Wernicke, H.-J. (Eds.) *Methanol: The Basic Chemical and Energy Feedstock of the Future*; Springer: Berlin/Heidelberg, Germany, 2014.

51. Ott, J.; Gronemann, V.; Pontzen, F.; Fiedler, E.; Grossmann, G.; Kersebohm, D.B.; Weiss, G.; Witte, C. "Methanol," in: Ullmann's Encyclopedia of Industrial Chemistry Enhanced Reader. *Ullmann's Encycl. Ind. Chem.* **2012**. [CrossRef]

52. Behrens, M.; Studt, F.; Kasatkin, I.; Kühl, S.; Hävecker, M.; Abild-Pedersen, F.; Zander, S.; Girgsdies, F.; Kurr, P.; Kniep, B.L.; et al. The Active Site of Methanol Synthesis over Cu/ZnO/Al$_2$O$_3$ Industrial Catalysts. *Science* **2012**, *336*, 893–897. [CrossRef]

53. Laudenschleger, D.; Ruland, H.; Muhler, M. Identifying the nature of the active sites in methanol synthesis over Cu/ZnO/Al$_2$O$_3$ catalysts. *Nat. Commun.* **2020**, *11*, 3898. [CrossRef]

54. Grabow, L.C.; Mavrikakis, M. Mechanism of Methanol Synthesis on Cu through CO$_2$ and COHydrogenation. *ACS Catal.* **2011**, *1*, 365–384. [CrossRef]

55. Studt, F.; Behrens, M.; Kunkes, E.L.; Thomas, N.; Zander, S.; Tarasov, A.; Schumann, J.; Frei, E.; Varley, J.B.; Abild-Pedersen, F.; et al. The Mechanism of CO and CO$_2$ Hydrogenation to Methanol over Cu-Based Catalysts. *ChemCatChem* **2015**, *7*, 1105–1111. [CrossRef]

56. Baltes, C.; Vukojevic, S.; Schuth, F. Correlations between synthesis, precursor, and catalyst structure and activity of a large set of CuO/ZnO/Al$_2$O3 catalysts for methanol synthesis. *J. Catal.* **2008**, *258*, 334–344. [CrossRef]

57. Spencer, M. Precursors of copper/zinc oxide catalysts. *Catal. Lett.* **2000**, *66*, 255–257. [CrossRef]

58. Behrens, M.; Brennecke, D.; Girgsdies, F.; Kißner, S.; Trunschke, A.; Nasrudin, N.; Zakaria, S.; Idris, N.F.; Hamid, S.B.A.; Kniep, B.; et al. Understanding the Complexity of a Catalyst Synthesis: Co-Precipitation of Mixed Cu,Zn,Al Hydroxycarbonate Precursors for Cu/ZnO/Al$_2$O$_3$ Catalysts Investigated by Titration Experiments. *Appl. Catal. A Gen.* **2011**, *392*, 93–102. [CrossRef]

59. Behrens, M.; Kasatkin, I.; Kühl, S.; Weinberg, G. Phase-Pure Cu,Zn,Al Hydrotalcite-like Materials as Precursors for Copper Rich Cu/ZnO/Al$_2$O$_3$ Catalysts. *Chem. Mater.* **2010**, *22*, 386–397. [CrossRef]

60. Gordillo, A.; Titlbach, S.; Futter, C.; Lejkowski, M.L.; Prasetyo, E.; Rupflin, L.T.A.; Emmert, T.; Schunk, S.A. High-Throughput Experimentation in Catalysis and Materials Science. *Ullmann's Encycl. Ind. Chem.* **2014**, 1–19. [CrossRef]

61. Titlbach, S.; Futter, C.; Lejkowski, M.; de Oliveira, A.L.; Schunk, S.A. High Throughput Technology: Exemplary Highlights of Advanced Technical Tools. *Chem. Ing. Tech.* **2014**, *86*, 1013–1028. [CrossRef]

62. Schunk, S.A.; Böhmer, N.; Futter, C.; Kuschel, A.; Prasetyo, E.; Roussière, T. High throughput technology: Approaches of research in homogeneous and heterogeneous catalysis. *Catalysis* **2013**, *25*, 172–215. [CrossRef]

63. Raudaskoski, R.; Niemelä, M.V.; Keiski, R.L. The effect of ageing time on co-precipitated Cu/ZnO/ZrO$_2$ catalysts used in methanol synthesis from CO$_2$ and H$_2$. In *Topics in Catalysis*; Springer: Dordrecht, The Netherlands, 2007; Volume 45, pp. 57–60.

64. Suh, Y.-W.; Moon, S.-H.; Rhee, H.-K. Active sites in Cu/ZnO/ZrO$_2$ catalysts for methanol synthesis from CO/H$_2$. *Catal. Today* **2000**, *63*, 447–452. [CrossRef]

65. Liu, X.-M.; Lu, G.Q.; Yan, Z.-F.; Beltramini, J. Recent Advances in Catalysts for Methanol Synthesis via Hydrogenation of CO and CO$_2$. *Ind. Eng. Chem. Res.* **2003**, *42*, 6518–6530. [CrossRef]

66. Huang, L.; Chu, W.; Long, Y.; Ci, Z.; Luo, S. Influence of Zirconia Promoter on Catalytic Properties of Cu–Cr–Si Catalysts for Methanol Synthesis at High CO Conversion in Slurry Phase. *Catal. Lett.* **2006**, *108*, 113–118. [CrossRef]

67. Raudaskoski, R.; Turpeinen, E.; Lenkkeri, R.; Pongrácz, E.; Keiski, R. Catalytic activation of CO_2: Use of secondary CO_2 for the production of synthesis gas and for methanol synthesis over copper-based zirconia-containing catalysts. *Catal. Today* **2009**, *144*, 318–323. [CrossRef]

68. Liu, X.-M.; Lu, G.; Yan, Z.-F. Nanocrystalline zirconia as catalyst support in methanol synthesis. *Appl. Catal. A Gen.* **2005**, *279*, 241–245. [CrossRef]

69. Wu, G.-S.; Mao, D.-S.; Lu, G.-Z.; Cao, Y.; Fan, K.-N. The Role of the Promoters in Cu Based Catalysts for Methanol Steam Reforming. *Catal. Lett.* **2009**, *130*, 177–184. [CrossRef]

70. Amenomiya, Y. Methanol synthesis from CO_2 + H_2 II. Copper-based binary and ternary catalysts. *Appl. Catal.* **1987**, *30*, 57–68. [CrossRef]

71. Denise, B.; Sneeden, R.P.A. Oxide-Supported Copper Catalysts Prepared from Copper Formate: Differences in Behavior in Methanol Synthesis from CO/H_2 and CO_2/H_2 Mixtures. *Appl. Catal.* **1986**, *28*, 235–239. [CrossRef]

72. Jeong, H.; Cho, C.H.; Kim, T.H. Effect of Zr and pH in the preparation of Cu/ZnO catalysts for the methanol synthesis by CO_2 hydrogenation. *React. Kinet. Mech. Catal.* **2012**, *106*, 435–443. [CrossRef]

73. Kanoun, N.; Astier, M.P.; Pajonk, G.M. Catalytic properties of new Cu based catalysts containing Zr and/or V for methanol synthesis from a carbon dioxide and hydrogen mixture. *Catal. Lett.* **1992**, *15*, 231–235. [CrossRef]

74. Brunauer, S.; Emmett, P.H.; Teller, E. Adsorption of Gases in Multimolecular Layers. *J. Am. Chem. Soc.* **1938**, *60*, 309–319. [CrossRef]